WEP Warwick Evans Publishing

Academic Journal of Management Science and Engineering

ISSN: 3080-9827 (Print), ISSN: 3080-9835 (Online) | Volume 1, Number 2, Year 2026
DOI: https://doi.org/10.62051/ajmse.v1n2.09
Journal homepage: https://ajomse.com

Numerical Simulation Study on Methane Transport and Dispersion in Soil under Different Leakage Locations

Xinxiong Lv

College of Pipeline Engineering, Xi'an Shiyou University, Xi'an, Shaanxi, 710065, China

ABSTRACT

To further investigate the influence of leakage direction in buried pipelines on gas diffusion within soil, this study develops a fluid–solid coupled numerical model based on the unified Darcy–Brinkman–Biot equations. The migration behavior of methane and crack evolution characteristics under single-side, adjacent double-side, and three-side leakage conditions are systematically simulated and compared. The results show that leakage direction directly determines the geometric configuration of soil cracks by altering the initial kinetic energy distribution and local gas pressure. As the number of leakage directions increases, the number of cracks increases significantly; however, due to energy dispersion, the length and width of individual cracks decrease. The three-side leakage condition exhibits the highest peak pressure in the initial stage (exceeding 3700 Pa), which drives the formation of a more complex and dispersed crack network. In addition, the evolution of methane concentration fields is highly consistent with crack development. As the main cracks penetrate the boundaries and form stable flow channels, the gas transport mechanism transitions from pore diffusion to rapid transport along crack pathways, exhibiting a pronounced channeling effect. These findings provide important numerical evidence for urban pipeline safety monitoring and risk assessment.

KEYWORDS

Buried Pipelines; Numerical Simulation; Crack Evolution; Fluid-Solid Coupling.

1. INTRODUCTION

With the continuous expansion of natural gas and hydrogen-blended pipeline networks, safety issues caused by pipeline leakage have become increasingly prominent [1]. During long-term operation, buried pipelines are prone to perforation failure due to corrosion or external forces [2–3], and such failures often exhibit distinct spatial orientation characteristics [4]. Once leakage occurs, the leakage direction directly affects the jet trajectory of the gas and the distribution of hazardous areas.

In buried environments, the interaction between leakage direction and the soil medium significantly alters gas diffusion behavior. Previous studies have shown that downward leakage is strongly influenced by soil resistance, resulting in a significantly smaller diffusion range compared to upward and lateral leakage. Moreover, gas diffusion rates and hazard ranges differ markedly under different leakage directions [2,5]. In confined spaces, leakage direction also affects gas accumulation characteristics and the response efficiency of detection systems [6–7]. To predict small-orifice leakage rates, Ebrahimi-Moghadam et al. [8] proposed an empirical correlation with an error of less than 5% based on two-dimensional simulation data for both above-ground and buried pipelines. Bezaatpour et al. [9] developed a three-dimensional CFD model that, under near-real soil conditions (including anisotropy, stratification, slope, and varying moisture content), revealed the leakage and dispersion characteristics of buried natural gas. Lyu et al. [10], through CFD simulations, identified

Content from this work may be used under the terms of CC BY-NC 4.0 licence (https://creativecommons.org/licenses/by-nc/4.0/).
Published by Warwick Evans Publishing.

the dominant roles of soil compaction, pipeline pressure, orifice size, and soil type in governing lateral methane diffusion and accumulation during buried pipeline leakage, and established a predictive model linking leakage rate to explosion hazard range.

Overall, leakage direction is a critical factor influencing gas migration patterns and hazard extents; however, quantitative studies remain relatively limited. Therefore, this study takes leakage direction as the key variable and employs numerical simulation methods [11–12] to systematically investigate the evolution of gas concentration distribution and hazard ranges under different leakage orientations, providing a reference for pipeline safety monitoring and risk prevention.

2. NUMERICAL METHODS

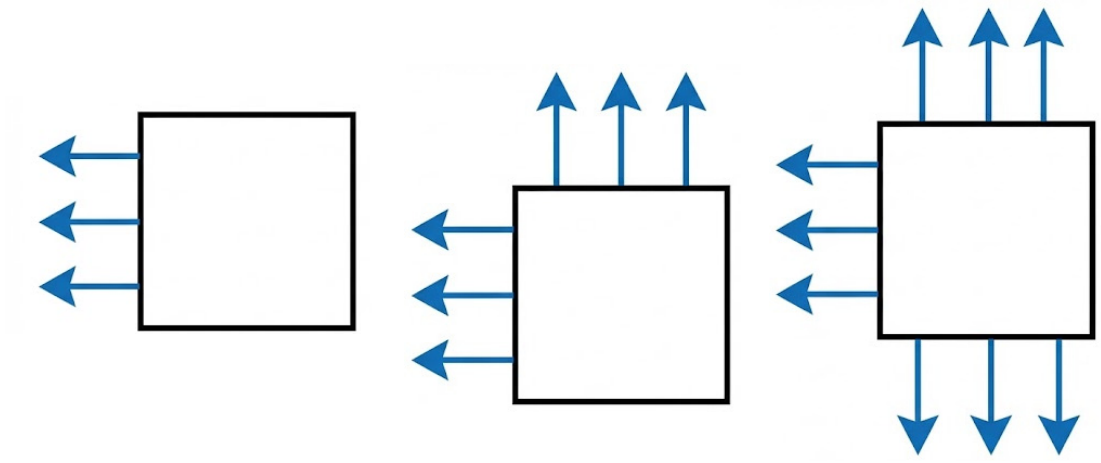
2.1. Physical Model and Mesh Generation

The physical model adopted in this study is a circular domain with a diameter of D = 300 mm. A square region with a side length of L = 5 mm is located at the center and serves as the leakage source, from which methane diffuses into the surrounding soil. For this model, a structured mesh is employed to discretize the computational domain, with a total of 196,256 cells and a uniform grid size of 0.6 mm. This ensures that concentration variations and soil response characteristics during gas diffusion can be captured with sufficient accuracy.

2.2. Mathematical Model

In this study, the fluid motion is described using a unified form of the Darcy–Brinkman–Biot equations. The Navier–Stokes equations are applied in solid-free regions, while Darcy's law is used to describe flow in porous media regions. Solid deformation is modeled based on Biot's theory, combined with an elastoplastic constitutive relationship. The momentum exchange between fluid and solid phases is coupled through a Darcy resistance term, and the methane leakage process is tracked using a convection–diffusion equation.

2.3. Mathematical Model



(a) (b) (c)

Figure 1. Schematic diagram of different leakage scenarios: (a) single-side leakage; (b) adjacent double-side leakage; (c) three-side leakage.

To investigate the influence of leakage velocity direction on methane diffusion and crack development, different velocity directions were assigned at the leakage boundary. The leakage velocity direction is defined as the outward normal direction of the leakage source boundary,

indicating gas injection from the source into the surrounding soil. To examine the differences in diffusion behavior under various directional conditions, three representative leakage scenarios were designed while keeping other parameters constant: single-side leakage, adjacent double-side leakage, and three-side leakage, as illustrated in Figure 1. In the single-side leakage case, the leakage velocity is applied only on the left boundary of the square leakage source, causing gas to diffuse horizontally to the left. In the adjacent double-side leakage case, leakage velocities are imposed on both the left and upper boundaries, resulting in gas leakage in both horizontal and vertical directions. In the three-side leakage case, leakage velocities are specified on the left, upper, and lower boundaries, allowing for the analysis of the coupled effects of multi-directional leakage on the diffusion process.In summary, this study conducts a series of numerical simulations by varying the leakage direction as a key factor, aiming to elucidate its influence on gas migration pathways, concentration distribution, and soil deformation patterns.

The specific parameters for the different simulation cases described above are listed in Table 1.

Table 1. Numerical simulation case setup for the study of leakage influencing factors

Case	Diffusion Coefficient (m^2/s)	Velocity Direction	Velocity (m/s)	Purpose
1	2×10^{-5}	Single-side leakage	1.04	To investigate the effect of natural gas leakage direction on methane diffusion behavior
2	2×10^{-5}	Adjacent double-side leakage	0.52	
3	2×10^{-5}	Three-side leakage	0.35	

Note: Except for the variables listed in the table, the remaining parameters are set as follows: the soil porosity follows a normal distribution ranging from 0.25 to 0.45 (mean value 0.35); the soil yield stress constant is 0.2; and the soil is assumed to be homogeneous sand–clay without natural cracks.

The mathematical model described in Section 2.2 is discretized within the computational domain using the finite volume method. The pressure–velocity coupling is solved using the PISO (Pressure Implicit with Splitting of Operators) algorithm. The convergence criterion for all physical variables at each time step is set to a residual less than 10^{-5}, with a maximum of 1000 iterations. In addition, a dynamic time-stepping strategy is adopted, and the Courant number is controlled below 0.1 during the computation to ensure numerical stability and accuracy.

3. RESULTS AND DISCUSSION

Figure 2 comprehensively presents the evolution of soil crack morphology within the computational domain at different time instants (t = 0.1 s, t = 0.5 s, and t = 2 s) under single-side leakage, adjacent double-side leakage, and three-side leakage conditions.

Under the single-side leakage condition, soil fracture exhibits a clearly directional development pattern. At t = 0.1 s, multiple microcracks first appear on the left side of the leakage orifice, indicating that gas initially preferentially diffuses in this region and induces localized changes in porosity. At t = 0.5 s, the crack morphology becomes more distinct, and the main crack continues to extend, while discontinuous fracture zones appear locally, reflecting spatial heterogeneity in pore structure evolution. By t = 2 s, the main crack penetrates the upper boundary, forming a stable gas escape channel, and the crack structure tends to stabilize. Under the adjacent double-side leakage condition, crack development exhibits characteristics of multi-directional interaction. At t = 0.1 s, microcracks first emerge in the upper-left region of the leakage orifice, corresponding to the dual-direction gas

diffusion paths. At t = 0.5 s, a crack network gradually forms, and the main crack shows a certain degree of curvature during propagation, indicating that its extension path is influenced by local variations in porosity distribution. By t = 2 s, the upper-left main crack fully penetrates the upper boundary and becomes the dominant channel, while cracks in the lower-left and right regions develop but do not fully connect, reflecting differences in crack development intensity across regions.

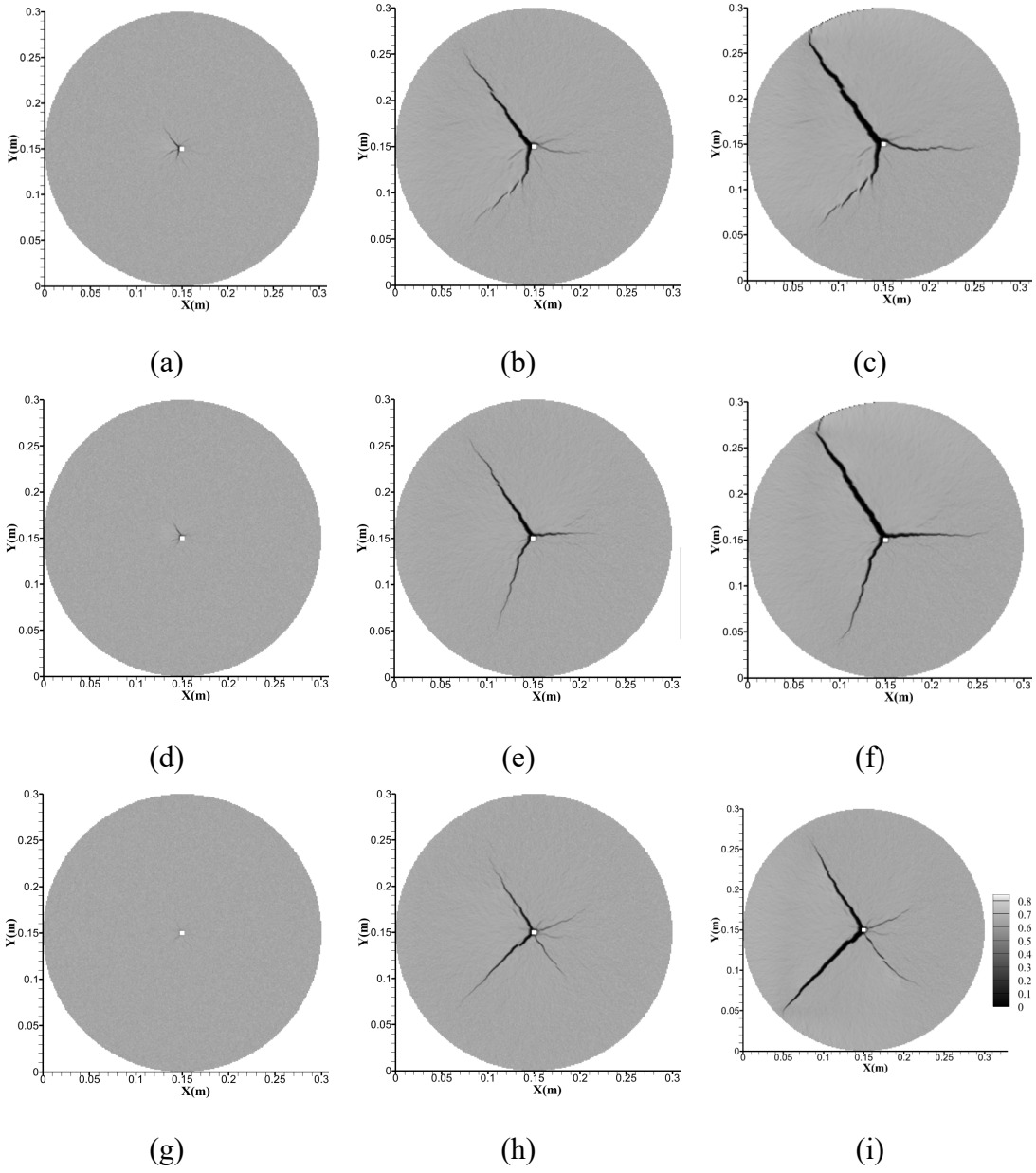


Figure 2. Comparison of soil crack morphology evolution in the computational domain under different leakage conditions: (a) single-side leakage t = 0.1 s; (b) single-side leakage t = 0.5 s; (c) single-side leakage t = 2 s; (d) double-side leakage t = 0.1 s; (e) double-side leakage t = 0.5 s; (f) double-side leakage t = 2 s; (g) three-side leakage t = 0.1 s; (h) three-side leakage t = 0.5 s; (i) three-side leakage t = 2 s.

Under the three-side leakage condition, crack evolution exhibits a more complex multi-channel behavior. At t = 0.1 s, no obvious cracks are observed in the computational domain, and the system remains close to its initial state. At t = 0.5 s, cracks in the upper-left and lower-left regions gradually develop into the primary fractures, while smaller secondary cracks appear on the right side, forming

a multi-channel coexistence pattern. By t = 2 s, the lower-left crack fully penetrates the boundary, the upper-left crack is close to breakthrough, and the right-side cracks remain relatively underdeveloped. Ultimately, the crack morphology exhibits a “butterfly-shaped” distribution, dominated by left-side fractures, reflecting spatial asymmetry in crack propagation and differences in porosity evolution.

To reveal the driving characteristics behind the differentiated evolution of the crack network, Figure 3 compares the temporal evolution of gas pressure at monitoring point 2 (located near a secondary crack, (0.259 m, 0.098 m)) under single-side, double-side, and three-side leakage conditions. Overall, the pressure under all three conditions exhibits a similar evolution pattern, characterized by a rapid increase in the early stage, followed by a gradual decrease and eventual stabilization.

In the initial stage of gas leakage (t < 0.3 s), since cracks have not yet formed, gas accumulates locally, leading to a rapid pressure increase. Among the three cases, the three-side leakage condition shows the highest peak pressure (exceeding 3700 Pa), while the single-side leakage case is relatively lower. After t = 0.5 s, as cracks gradually develop and connect with the boundaries, gas diffusion pathways begin to form, and the pressure in all cases decreases significantly. By t = 2 s, the crack morphology becomes stable, and the pressure stabilizes within the range of 2000–2400 Pa. The evolution of gas pressure is consistent with the process of crack initiation, propagation, and penetration. The higher initial pressure under the three-side leakage condition promotes multidirectional gas diffusion, thereby facilitating the full development of the crack network, which corresponds to the more complex crack morphology observed in this case. The analysis indicates that different leakage boundary conditions influence crack development range and morphology by affecting gas pressure distribution and diffusion processes.

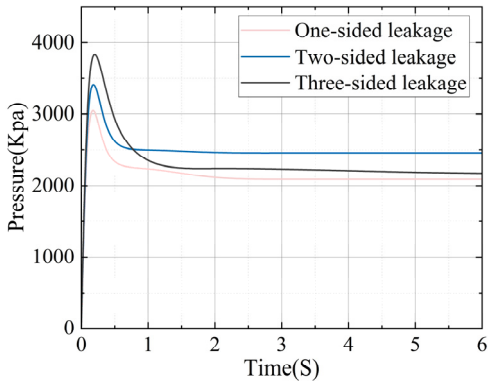


Figure 3. Comparison of pressure–time responses at monitoring point 2 under single-side, double-side, and three-side leakage conditions.

Table 2 presents the number, length, width, and inclination angle relative to the horizontal direction of cracks under different leakage orientations. The results show that as the number of leakage directions increases, the total number of cracks also increases, indicating that multi-directional leakage promotes gas pressure accumulation along more pathways and facilitates crack initiation. In contrast, the maximum length and width of individual cracks decrease, suggesting that the gas energy is dispersed across multiple directions, thereby limiting crack propagation and lateral expansion. The variation in crack inclination angles relative to the horizontal direction indicates that multi-directional leakage alters the spatial orientation of crack development, causing the overall crack pattern to deviate from the initial leakage direction or form a more complex propagation path. Therefore, leakage direction influences not only the number and size of cracks by regulating local pressure distribution and stress concentration, but also determines the spatial configuration of cracks, thereby exerting a significant impact on methane migration pathways and diffusion characteristics.

Figure 4 comprehensively presents the evolution characteristics of the methane concentration field within the computational domain at different time instants (t = 0.1 s, t = 0.5 s, and t = 2 s) under single-side, adjacent double-side, and three-side leakage conditions. Under the single-side leakage condition, methane concentration is primarily controlled by the dominant flow channel.

Table 2. Effects of different leakage directions on crack development characteristics and spatial distribution.

Leakage condition	Number of cracks	Maximum crack length (mm)	Maximum crack width (mm)	Inclination angle to horizontal (°)
Single-side leakage	3	110.7	6.4	125.8
Adjacent double-side leakage	3	108.5	5.8	122.8
Three-side leakage	4	106.1	4.4	-135.4

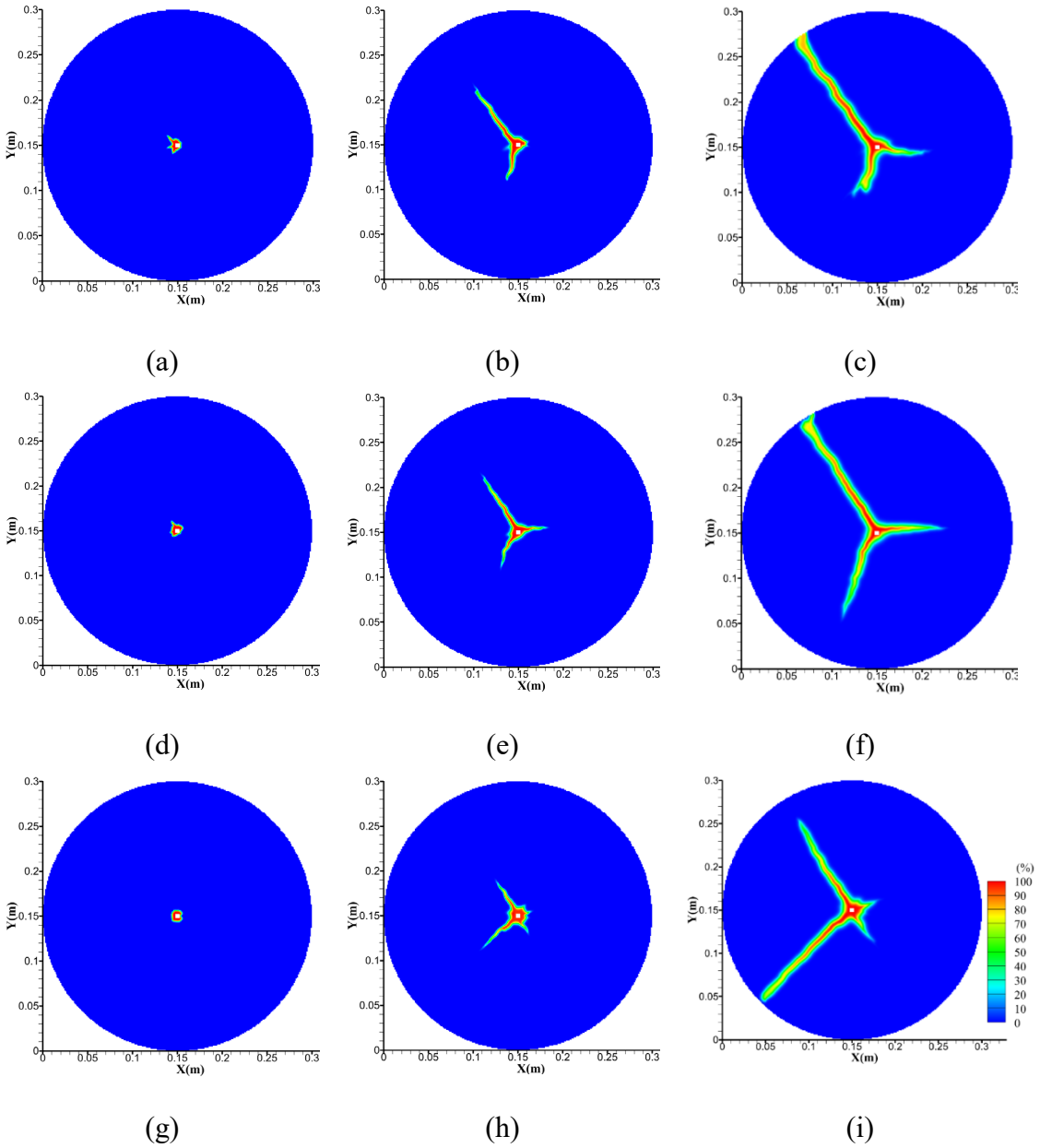


Figure 4. Comparison of methane concentration field evolution within the computational domain under different leakage conditions: (a) single-side leakage t = 0.1 s; (b) single-side leakage t = 0.5 s; (c) single-side leakage t = 2 s; (d) double-side leakage t = 0.1 s; (e) double-side leakage t = 0.5 s; (f) double-side leakage t = 2 s; (g) three-side leakage t = 0.1 s; (h) three-side leakage t = 0.5 s; (i) three-side leakage t = 2 s.

At t = 0.1 s, gas is concentrated around the leakage orifice, and the local high-concentration region exhibits a spike-like pattern, reflecting the directional nature of the initial jet. At t = 0.5 s, the concentration spreads directionally along the crack channel, and the morphology of the high-concentration region is consistent with the crack geometry. At t = 2 s, methane is mainly confined within the main crack, and transport is dominated by the crack pathway, while diffusion through soil pores becomes weak.

Under the adjacent double-side leakage condition, gas flow exhibits a superposition effect of multiple directions. At t = 0.1 s, concentration is mainly accumulated near the leakage source, with a local protrusion appearing along the upper-left crack. At t = 0.5 s, the high-concentration region migrates along the upper-left main crack, and the concentration gradient closely matches the crack morphology. At t = 2 s, the highest concentration occurs within the upper-left main crack, while weaker diffusion zones appear in the lower-left and right regions, indicating competition among different transport pathways and the eventual formation of a dominant flow channel.

Under the three-side leakage condition, gas migration exhibits multi-channel distribution and competition. At t = 0.1 s, high concentration remains concentrated around the leakage source, with no obvious migration pathways formed. At t = 0.5 s, irregular high-concentration zones develop along the upper-left and lower-left cracks, reflecting the influence of crack development and pore structure evolution on gas transport. At t = 2 s, methane is mainly concentrated in the two main cracks on the upper-left and lower-left sides, with the lower-left channel showing more pronounced development, while the right-side region only exhibits localized concentration increases. This indicates that under multi-directional leakage conditions, gas migration is dominated by main crack channels, accompanied by limited secondary diffusion.

4. CONCLUSION

Variations in leakage direction alter the initial momentum distribution and diffusion pathways of gas entering the soil, thereby directly affecting the spatial configuration of crack development. Under multi-directional leakage conditions, the number of cracks increases significantly, while the scale of individual cracks decreases. The crack propagation paths become more dispersed and disordered, and spatial heterogeneity is enhanced.

As the main cracks gradually form and develop stably, their controlling effect on gas migration pathways becomes increasingly pronounced. Gas preferentially migrates and rapidly diffuses along crack channels, while transport in non-cracked regions is significantly restricted. Overall, the concentration distribution exhibits a strong channelization effect.

REFERENCES

[1] Kan Yiwei, Gu Haowen. Numerical simulation study on natural gas pipeline leakage and dispersion [J]. Value Engineering, 2022, 41(36): 124–126.

[2] Liu Gang, Wang Xin, Chen Duo, et al. Influence of soil properties on the dispersion behavior of hydrogen-blended natural gas pipeline leakage [J]. Oil & Gas Chemical Industry, 2024, 53(05): 33–45.

[3] Jin Zengfeng, Li Jun, Xin Xin, et al. Study on influencing factors of leakage and dispersion of buried hydrogen-blended natural gas pipelines [J]. Oil and Gas & New Energy, 2025, 37(06): 38–45.

[4] Song Xiaojun, Liang Longgui, Chen Qingguo, et al. Failure analysis of buried natural gas pipelines [J]. Petroleum Tubular Goods & Instruments, 2024, 10(02): 76–80.

[5] Guo Yiwen, Gong Sifan, Wang Pengfei. Numerical simulation of buried natural gas pipeline leakage based on FLUENT [J]. Mining Engineering Research, 2024, 39(01): 35–40.

[6] Liu Baodong, Liao Zhihua, Li Ming, et al. Study on gas dispersion characteristics of natural gas leakage in underground utility tunnels [J]. Journal of University of Shanghai for Science and Technology, 2025, 47(01): 54–60.

[7] Shen Jing, Du Shengqun, Li Xinyue, et al. Review on leakage dispersion and explosion of natural gas in underground utility tunnels [J]. Journal of Catastrophology, 2025, 40(01): 129–134.

[8] A. Ebrahimi-Moghadam, M. Farzaneh-Gord, M. Deymi-Dashtebayaz, Correlations for estimating natural gas leakage from above-ground and buried urban distribution pipelines, J. Nat. Gas Sci. Eng. 34 (2016) 185–196.

[9] J. Bezaatpour, E. Fatehifar, A. Rasoulzadeh, CFD investigation of natural gas leakage and propagation from buried pipeline for anisotropic and partially saturated multilayer soil, J. Clean. Prod. 277 (2020) 123940.

[10] Lyu, S., Huang, X., Ma, X., et al., CFD modeling of leakage and dispersion characteristics of buried natural gas pipelines - part 1: Numerical simulation, Int. Commun. Heat Mass Transf. 172 (2026) 110351.

[11] Zhao Wei, Deng Bofan, Ren Yiqun, et al. Study on leakage dispersion characteristics of buried hydrogen-blended natural gas pipelines [J]. Gas & Heat, 2025, 45(06): 1–8.

[12] Qian Hao. Experimental study on natural gas leakage dispersion and optimization of Gaussian prediction models [J]. Natural Gas Industry, 2024, 44(07): 154–164.